Correspondence to:
S. Lovejoy,
lovejoy@physics.mcgill.ca

On Mars too expect macroweather

Shaun Lovejoy[1], J.-P. Muller[2], and J. P. Boisvert[1]

[1]Department of Physics, McGill University, Montreal, Quebec, Canada, [2]Mullard Space Science Laboratory, Department of Space and Climate Physics, Dorking, UK

Abstract Terrestrial atmospheric and oceanic spectra show drastic transitions at $\tau_w \approx 10$ days and $\tau_{ow} \approx 1$ year, respectively; this has been theorized as the lifetime of planetary-scale structures. For wind and temperature, the forms of the low- and high-frequency parts of the spectra (macroweather and weather) as well as the τ_w can be theoretically estimated, the latter depending notably on the solar-induced turbulent energy flux. We extend the theory to other planets and test it using Viking lander and reanalysis data from Mars. When the Martian spectra are scaled by the theoretical amount, they agree very well with their terrestrial atmospheric counterparts. We discuss the implications for understanding planetary fluid dynamical systems.

1. Introduction

Atmospheric wind spectra undergo some kind of transition at scales of $\tau_w \approx 2$–10 days. First ascribed to "migratory pressure systems of synoptic weather map scale" [*Panofsky and Van der Hoven*, 1955; *Van der Hoven*, 1957], the corresponding pressure feature was termed the "synoptic maximum" by *Kolesnikov and Monin* [1965] and *Panofsky* [1969]. More recently, *Vallis* [2010] attributed it to baroclinic instabilities and estimated the timescale by the Eady growth rate τ_{Eady} (≈ 4 days in midlatitudes). Over time, the view evolved that the spectrum is essentially that of an Ornstein-Uhlenbeck process, i.e., of a Gaussian white noise at frequencies $\omega < (\tau_w)^{-1}$ and the integral of a white noise at frequencies $\omega > (\tau_w)^{-1}$ [e.g., *AchutaRao and Sperber*, 2006]; this is the basis of the stochastic linear forcing approach [*Hasselmann*, 1976; *Penland*, 1996; *Newman et al.*, 2003; *Sardeshmukh and Sura*, 2009] and the critique in *Lovejoy and Schertzer* [2013, p. 371].

Alternatively, the transition was theorized as separating two scaling regimes: a high-frequency weather regime and a much flatter (but not completely flat) low-frequency "spectral plateau" [*Lovejoy and Schertzer*, 1986]. More recently, building on a body of work showing that atmospheric spatial scaling is highly anisotropic and extends up to planetary scales, *Lovejoy and Schertzer* [2010] argued that the transition scale τ_w was simply the lifetime of planetary-scale structures and could be estimated from first principles using the (turbulent) energy flux ε induced by solar forcing. This regime was initially called "low-frequency weather" regime since its statistics are determined by a succession of planetary weather structures. With the help of turbulence-based cascade models, the transition was theorized as a "dimensional transition": at timescales shorter than τ_w, all the spatial weather degrees of freedom are important, whereas at longer timescales, they are progressively averaged out, becoming effectively "quenched." Ultimately, at scales longer than $\tau_c >> \tau_w$, new slow climate processes become important. The ocean is also a stratified turbulent system—but with $\tau_{ow} \approx 1$ year; *Lovejoy and Schertzer* [2012] argued that this could be explained by the same mechanism but with much smaller ε (see Figure 2a).

In a recent review [*Lovejoy and Schertzer*, 2013; see also *Lovejoy*, 2013, chapter 10], it was pointed out that the nature of the transition could most easily be grasped using fluctuations $\Delta T(\Delta t)$, whose scaling exponent of the mean, H, changes sign at τ_w. Ignoring intermittency, the critical value $H = 0$ corresponds to $\beta = 1$ where $E(\omega) \approx \omega^{-\beta}$ is the spectrum. In the weather regime ($\Delta t < \tau_w$ and $H > 0$; $\beta \geq 1$), fluctuations grow as $\Delta T(\Delta t) \approx \Delta t^H$, and at scales $\Delta t > \tau_w$ they decrease ($H < 0$; $\beta \leq 1$). This means that while plots of $T(t)$ for $\Delta t < \tau_w$ tend to "wander" like a drunkard's walk, for $\Delta t > \tau_w$ successive fluctuations tend to cancel each other out. Since unforced global climate models and cascade models—both based on weather-scale physics—reasonably reproduce these statistics, the designation "macroweather" was proposed. While this "canceling" behavior corresponds to the usual idea of climate as the state to which averages of "weather" converge, the convergence is arrested at a scale τ_c (≈ 10–30 years, ≈ 50–100 years: industrial and preindustrial eras, respectively) beyond which lower frequency processes lead again to increasing ($H > 0$) fluctuations. It was therefore argued that—to

paraphrase the dictum—macroweather (not climate) is "what you expect," while at longer scales, it is the climate "that you get."

If the scaling trichotomy of weather—macroweather—climate is correct, then this has fundamental implications for understanding atmospheric dynamics including forecasting. It requires us to replace the classical focus on narrow range quasiperiodic processes with one based on wide range space-time scaling processes. Indeed, *Lovejoy* [2014] showed that the quasiperiodic "mental picture" is based on an iconic and still frequently cited spectrum by *Mitchell* [1976] that is wrong by a factor of 10^{14}–10^{15}. Indeed, it is increasingly clear that only a small fraction of atmospheric variability is in quasiperiodic processes and that almost all is in the scaling regimes.

Such a reversal of the roles of foreground and background is sufficiently important that it requires much empirical support. However, at present, the key weather-macroweather regimes and transitions are empirically supported by only two examples—both terrestrial—our atmosphere and ocean. Since the physics is hypothesized to depend on turbulent energy fluxes [see *Lovejoy and Schertzer*, 2013, chapters 2, 4, and 6], we expect that the same behavior should be observed on other planets. In this paper, we consider the nonterrestrial planet with the best data: Mars.

The use of turbulence laws up to planetary scales—even if nonclassical due to anisotropy and intermittency —may seem surprising in view of the usual approach to the large-scale Martian circulation [*Hollingsworth and Barnes*, 1996; *Read and Lewis*, 2004; see also *Leovy*, 2001] that relies on quasi-linear analyses including diurnal tides, the interaction between planetary waves, and the topography. However, an analogous apparent contradiction appears in tropical meteorology, which—while often understood in similar type terms— nevertheless well respects high-level statistical laws showing their compatibility with mechanistic, deterministic explanations [*Pinel et al.*, 2014a; *Pinel and Lovejoy*, 2014]. Here thanks to Martian reanalyses, we have directly confirmed the multiplicative nature of the dynamical fluxes as well as the rough Kolmogorov horizontal spectra (although with artifacts similar to those of terrestrial reanalyses [*Lovejoy and Schertzer*, 2011]). Finally, although there are several papers on Martian boundary layer turbulence [e.g., *Tillman et al.*, 1994; *Izakov*, 2001; *Martinez et al.*, 2009], these are not directly relevant to the temporal spectral properties discussed here.

2. Estimating the Outer Timescales of Planetary Weather

2.1. The Basic Theoretical Framework, the Earth

Due to gravity, the vertical and horizontal scalings of atmospheric fields are generally quite different, leading to increasing stratification at larger and larger scales, but without introducing a characteristic scale. The resulting $23/9 \approx 2.56$ D model [*Schertzer and Lovejoy*, 1985] is characterized by the horizontal dynamics (wind field) being dominated by turbulent energy fluxes ($\varepsilon = -\partial v^2/\partial t$ with dimensions $m^2/s^3 = W/kg$) and the vertical dynamics by buoyancy variance fluxes (see the reviews of *Lovejoy and Schertzer* [2010, 2013, chapter 6]). This implies that for two points separated by horizontal distance Δx, the wind difference Δv obeys Kolmogorov scaling:

$$\Delta v \approx \varepsilon^{1/3} \Delta x^{1/3} \tag{1}$$

If Δx is the largest great circle distance ($= \pi r$ where r is the planet's radius), then Δv is the typical antipodes velocity difference, it is also the typical large-scale velocity V_w:

$$V_w \approx \varepsilon^{1/3} L_w^{1/3}; \quad L_w = \pi r \tag{2}$$

("w" indicates weather, L_w for the spatial weather scale). Since L_w is the outer space scale of the planetary weather, the corresponding lifetime is the outer weather timescale τ_w:

$$\tau_w = \frac{L_w}{V_w} = \frac{\pi r}{V_w} = L_w^{2/3} \varepsilon^{-1/3} \approx \left(\frac{\pi^2 r^2}{\varepsilon} \right)^{1/3} \tag{3}$$

Therefore, to find τ_w given the planet's radius r, we only need ε via measurements or from first principles. For example, varying somewhat with latitude and altitude, *Lovejoy and Schertzer* [2010] found $\varepsilon \approx 10^{-3}$ W/kg, and in the ocean surface layer, *Lovejoy and Schertzer* [2012] found $\varepsilon \approx 10^{-8}$ W/kg. These values lead to $\tau_w \approx 10$ days and $\tau_{ow} \approx 1$ year, respectively (see Figure 2a).

Table 1. Basic Planetary Constants and Ratios[a]

	Earth	Mars	Ratio (Mars/Earth)
Δp	10^5 N/m^2	500 N/m^2	5×10^{-3}
Radius (r)	6.37×10^6 m	3.39×10^6 m	0.53
Distance from Sun (R)	1.50×10^{11} m	2.28×10^{11} m	1.52
Mass (m)	6.0×10^{24} kg	6.42×10^{23} kg	1.07
Albedo (α)	0.30	0.11	0.37
ε (W/kg)	1.0×10^{-3}	0.04	40
τ_w (s)	7.3×10^5	1.5×10^5	0.21
τ_w (local days)	8.4	1.8	0.21
V_w (m/s)	27	70.3	2.60

[a]Note that 1 sol = 1.027 Earth days and 1 Martian year = 669 sols. The parameters were estimated from equations (5) and (6) assuming $e_e = e_p = 0.04$. The data for the first five rows were taken from Wikipedia; for the others, see the paper.

In order to derive ε, τ_w from first principles, let the total solar insolation be I; the mean power absorbed per unit area is $F = I \frac{(1-\alpha)}{4}$; α is the mean albedo, and the factor ¼ comes from averaging over angles and the diurnal cycle. If we assume that the dynamics distribute this over an atmospheric column of thickness Δp, then the mass per unit area is $M = \frac{\Delta p}{g}$ where g is the local acceleration of gravity. The energy flux per mass is thus

$$\varepsilon = e\frac{F}{M} = \frac{eI(1-\alpha)g}{4\Delta p} \tag{4}$$

where e is the fraction of solar energy converted into kinetic energy, the efficiency.

For the Earth, $I = 1.365 \times 10^3$ W/m^2, $\Delta p = 10^5$ N/m^2, $g = 9.81$ m/s^2, and $\alpha = 0.30$. Old estimates of e were ≈ 0.02 [*Monin*, 1972]; from the modern value of $\varepsilon \approx 1.0 \times 10^{-3}$ W/kg we infer $e \approx 0.04$. Using equation (3), we obtain

$$\tau_w = \left(\frac{4\Delta p \pi^2 r^2}{eI(1-\alpha)g} \right)^{1/3} \tag{5}$$

see Table 1. If we directly estimate τ_w from the position at which the spectrum flattens, for temperature we find a latitudinal variation from about 7 days at high latitudes to 15 days near the equator and about half of this for precipitation [*Lovejoy and Schertzer*, 2013, Figure 8.5c].

2.2. Other Planets

The simplest way to estimate values for the other planets is to scale them to the Earth (subscripts "p" and "e," respectively) from equation (4)

$$\frac{\varepsilon_p}{\varepsilon_e} = \left(\frac{\Delta p_e}{\Delta p_p} \right) \left(\frac{r_e}{r_p} \right)^2 \left(\frac{R_e}{R_p} \right)^2 \left(\frac{m_p}{m_e} \right) \left(\frac{e_p}{e_e} \right) \left(\frac{1-\alpha_p}{1-\alpha_e} \right) \tag{6}$$

where the ratio of the incoming solar radiation is estimated by scaling the terrestrial value by the square of the ratio of the mean distances from the Sun (R_e, R_p), and the ratio of surface gravities is expressed in terms of the planetary masses (m) and radii (r). Lacking a better theory, we took $e_p = e_e = 0.04$. Using the same substitutions, Table 1 shows the basic parameters for the Earth and Mars and the corresponding ε, τ_w, and V_w estimates.

2.3. Temporal Scaling and Spectra

A consequence of the horizontal scaling is that V_w is the velocity needed to convert space to time; this is verified using satellite data in *Pinel et al.* [2014b]. In this case we have

$$\Delta v \approx (\Delta x \varepsilon)^{1/3} = (V_w \Delta t \varepsilon)^{1/3} = \left((L_w \varepsilon)^{1/3} \varepsilon \Delta t^{1/3} \right) = \varepsilon^{4/9} L_w^{1/9} \Delta t^{1/3} \tag{7}$$

with spectrum

$$E_V(\omega) \approx \left\langle \varepsilon^{8/9} \right\rangle L_w^{8/9} \omega^{-5/3} \tag{8}$$
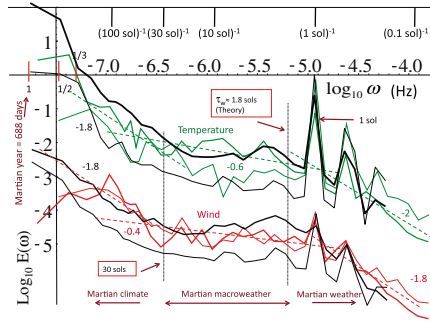
Figure 1. The Viking 1 and 2 (thin: 22°N, thick: 48°N) temperature and wind spectra (green and red) averaged over 10 bins per order of magnitude (logarithmically spaced); the units are K² h and m² s⁻² h, respectively; the wind spectra have been displaced downward by 2 orders of magnitude for clarity. The pairs of black lines are from the reanalyses at corresponding latitudes (thin: 20°N, thick: 50°N). The data series were cubically detrended to remove much of the annual cycle. The three red ticks at the far left indicate the Martian year and harmonics at a half and a third of a year; these are the only frequencies significantly affected by the detrending. The dashed reference lines are the terrestrial values with slopes indicated [*Lovejoy and Schertzer*, 2013, chapters 8 and 10]. Also indicated are the three scaling regimes; the climate regime (below about (30 days)⁻¹) is not clear since the spectrum rises due to the poorly resolved annual cycle.

where "$<.>$" indicates ensemble average. The corresponding temperature formula is less clear, but the standard "passive scalar" formula is still the best available [*Obukhov*, 1949; *Corrsin*, 1951]:

$$\Delta T \approx \chi^{1/2}\varepsilon^{-1/6}\Delta x^{1/3} \qquad (9)$$

where χ is the passive scalar variance flux ($\chi = -\partial T^2/\partial t$). Again, using $\Delta x = V_w \Delta t$, we obtain

$$\Delta T \approx \chi^{1/2}\varepsilon^{-1/18}L_w^{1/9}\Delta t^{1/3} \qquad (10)$$

and

$$E_T(\omega) \approx \left\langle \chi\varepsilon^{-1/9}\right\rangle L_w^{2/9}\omega^{-5/3} \qquad (11)$$

The weather regime scaling is associated with space-time cascade processes operating up to scales of at least 5000 km; evidence from satellite data, reanalyses, aircraft data, and weather models is reviewed in *Lovejoy and Schertzer* [2013, section 10.1]; using Martian reanalyses below, we confirm that they also hold up to about a quarter of the circumference. If these cascades are extended to long times (e.g., well beyond τ_w), they imply macroweather

scaling with β weakly dependent on the overall scale range but typically $0.2 \lesssim \beta \lesssim 0.4$. If the corresponding ocean cascade is taken into account, one can obtain $\beta \approx 0.6$ [see *Lovejoy and Schertzer*, 2013, p. 378].

3. The Data and Analysis

In order to test the theory, we need data spanning the transition scale so that we can estimate τ_w and confirm that the Martian and terrestrial spectra are close. From Table 1, we see that for Mars this implies data of resolutions of at least several hours with series lasting of the order of a month or more; the optimum data were from the two Viking landers. The short mission duration for Pathfinder, the irregular interruptions of data collection from Phoenix, the absence of anemometers on Spirit and Opportunity, and the lack of data available from Curiosity (when this analysis started) make these more recent Martian lander data less useful.

The Viking landers provided measurements of both temperature and wind speed at a height of 1.5 m every 59.2 min. Wind speed was measured using two hot-film anemometers, and ambient temperature was measured using three thermocouples connected in parallel. The error on wind measurements is estimated to be 10%, and on temperature ≈ 1.5 K for Lander 1, ≈ 3 K for Lander 2 [*Hess et al.*, 1977]. The Viking 1 lander made 8325 continuous measurements (350 Martian days or "sols"); the Viking 2 set was longer but had gaps. We used a 13,794 data point long sequence (574 sols) with only 440 missing points—sufficiently few that we could use linear interpolation for the gaps.

Figure 1 shows the resulting (full range) of the Viking 1 and 2 spectra (with cubic detrending to remove much of the effect of the annual cycle), and Figure 2a shows a superposition of the detrended temperature spectrum—shifted to the left by the theory value $-\log_{10}\tau_{w,\,Mars}/\tau_{w,\,Earth} = 0.68$ (Table 1), with only an extra shift of 0.1 needed to obtain excellent Mars/Earth overlap—at least for frequencies above $\approx$ (30 sols)⁻¹. At lower frequencies, there is a marked spectral increase due either to the incompletely resolved annual spike (see the red ticks on the axis at the left) or to the beginning of the Martian climate—or to both (the Earth climate reference slope −1.8 that starts at $\approx$ (50 years)⁻¹ has been added).
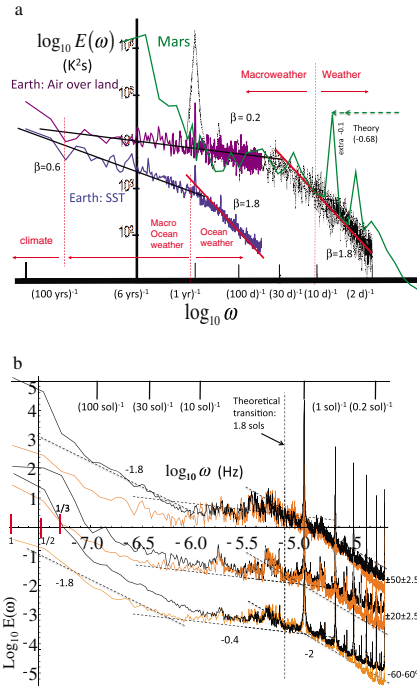
Figure 2. (a) A comparison of the Martian temperature spectrum (cubically detrended, green, from Viking 2 (Figure 1), shifted left by the theoretical amount (−0.68) and an additional 0.1 for a better fit), superposed on an Earth air over land spectrum (monthly data, 100 years long, purple, left) and sea surface temperature (SST, blue, bottom left). Also shown (right, black, reproduced from *Lovejoy and Schertzer* [1986]) is the spectrum of daily temperatures from Macon France. The red reference lines have slopes −1.8. The weather, macroweather regimes are indicated; the climate regime (frequencies $< \approx (50 \text{ years})^{-1}$) is only hinted here (see *Lovejoy and Schertzer* [2013] for a discussion and review of this and other evidence). Adapted from *Lovejoy and Schertzer* [2012, Figure 4]. (b) Martian reanalysis: 660 sols of data sampled every 1/12 sol, starting at year 24 longitude 141°, (May 1999) sigma level 0.995 (near surface). Black is temperature; orange is the zonal wind, units: K^2 h and $(\text{m/s})^2$ h. The dashed vertical line is the theoretical weather/macroweather transition. The 20° latitude pair has been shifted upward by 2 orders of magnitude, the 50° latitude by 4 orders. The bottom pair is for the entire planet between ±60° latitude. The dashed lines have reference slopes as indicated. Red lines indicate Martian year and fractions thereof. To quantify the series to series spread/error, each individual spectrum was averaged over logarithmically spaced frequency bins as in Figure 3. The standard deviations of the $\log_{10}$ of the bin- (frequency range) averaged spectra were found to decrease roughly linearly from ±0.8 to ±0.4 from low to high frequency (±60° curves), from ±0.7 to ±0.2 (50° curves), and ±0.6 to ±0.2 for (20° curves), with very similar spreads for temperature and wind.

In spite of averaging the spectrum over logarithmical space frequency bins, the result is still very noisy; we therefore compared it to spectra of the zonal wind estimated from Martian reanalyses [*Montabone et al.*, 2011] at the near-surface reanalysis level, using data every 1/12 sol for 660 sols (Figures 1 and 2b). Due to averaging the spectra over many pixels, the spectral transitions and slopes are quite clear (Figure 2b) and the agreement with the Viking data (Figure 1) is striking. Notice that even the latitudinal variations are well reproduced by the reanalyses. From the reanalysis it was possible to verify that the scaling is accurate with $1.5 < \beta < 2.4$ at least for levels in the upper 70% of the atmosphere. Although these exponents are compatible with ε domination in the horizontal (Kolmogorov scaling), there are similar north-south/east-west anisotropy issues and artifacts as in terrestrial reanalyses [*Lovejoy and Schertzer*, 2011], and a full discussion is outside our scope. As expected, the large-scale V_w and ε increased at higher and higher levels, respectively: (28, 34, 55, and 87) m/s and (0.005, 0.01, 0.02, and 0.08) W/kg for sigma pressure levels (0.73, 0.46, 0.12, and 0.006), respectively, close to the theoretical estimates in Table 1; see also the somewhat larger estimates under (extreme) convective conditions: (0.20, 0.02, and 0.17) W/kg from, respectively, Viking 1 and 2 and Pathfinder data [*Martinez et al.*, 2009].

In order to make a slightly different Earth/Mars comparison, we also analyzed two (continental U.S.) weather stations: Darrington, Washington, and Panther Creek, Texas (latitudes 48° and 29°). The data were from the U.S. Climate Reference Network (USCRN) for both wind and temperature (also at 1.5 m), at comparable latitudes to the Landers (48°, 22° for Lander 2 and 1, respectively). There were no interruptions in the data over a yearlong series (2008). Wind speed was measured with a three-cup anemometer and temperature with a platinum resistance thermometer. The errors were 1.5% and 0.04% (wind and temperature) [see *Diamond et al.*, 2013].

In our final comparison (Figures 3a and 3b), we therefore broke both the Earth and Mars series into segments, each 30 local days
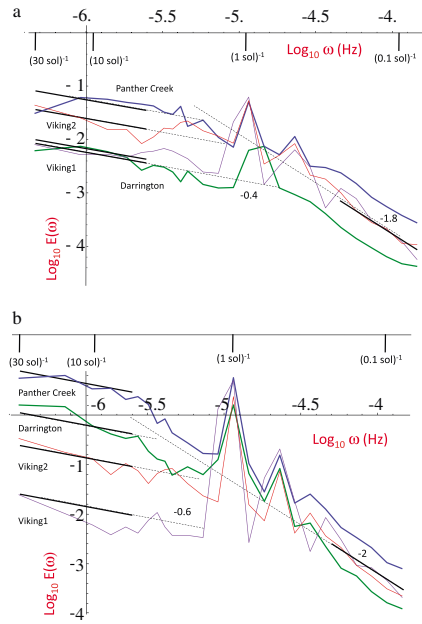
Figure 3. (a) Spectra for Earth and Martian surface temperatures from Panther Creek, Texas (blue), Darrington, Washington (green), Viking 1 (purple), and Viking 2 (red). The Earth stations have been offset (upward) by 1 order of magnitude for clarity. The reference lines have slopes -0.4 (low frequencies) and -1.8 (high frequencies). The units are K^2 h. To quantify the series to series spread/error, each of these frequency bin-averaged spectra was used to determine the standard deviations of the $\log_{10}$ spectral densities about the means. At the low frequencies the variations were between ± 0.6 and ± 0.8, whereas at the highest frequencies the variations were between ± 0.2 and ± 0.4 (decreasing roughly linearly from the low frequencies; the higher latitudes had the higher spreads). (b) The same as Figure 3a except for the wind data. The Earth stations have been offset (upward) by 1 order of magnitude for clarity. The reference lines have slopes -0.6 (low frequencies) and -2 (high frequencies). The units are K^2 m^2 s^{-2}. The spreads of the individual spectra about the means were close to those of the temperatures in Figure 3a.

long, treating each as a separate realization. Averaging spectra over segments improves the spectral statistics while simultaneously avoiding most of the Viking 2 gaps. The results are shown in Figure 3a (temperatures) and Figure 3b (wind). The diurnal variation and harmonics—especially for the Viking temperatures—are very strong making the interpretation of the spectra in the vicinity of the Martian day nontrivial. We found that the amplitude of the diurnal cycle varied considerably from one Martian season to another so that there is no simple way to remove the cycle. The strong cycle also prevented us from using real space (fluctuation and wavelet) analysis since this would "spread" the diurnal cycle over a wide range of scales. Consequently, we plotted low- and high-frequency macroweather and weather reference lines over the ranges $(30\ \text{sols})^{-1}$ to $(6\ \text{sols})^{-1}$ and $(1/4\ \text{sol})^{-1}$ to $(1/12)^{-1}$, respectively, i.e., we avoided the range near a sol.

From the figures, we see that for Earth there is considerable variation in the spectra between the two locations but that this is comparable to the variation between the two Lander spectra. The reference lines had slopes that were close to the Earth theory (equations (8) and (11): $\beta = 5/3$) but were a little steeper (for the weather regime: $\beta = 1.8$ and 2, for macroweather: $\beta = 0.4$ and 0.6); these were close to the empirical Earth values. Note that these correspond to scaling exponents $H \approx -0.3$ and -0.2 and imply a high degree of stochastic predictability.

4. Conclusions

Atmospheric variability has traditionally been viewed as a sequence of quasiperiodic (narrow band) processes superposed on an uninteresting more or less white noise continuum "background" spectrum. However, both numerical models and modern data show that this picture is radically in error and that a realistic framework consists rather of wide-range scaling processes with several small quasiperiodic perturbations. The best documented scaling processes are in the weather and macroweather regimes, characterized by growing ($H > 0$) and decreasing ($H < 0$) fluctuations. First principle turbulence-based theory predicts both the spectral exponents and—when combined with solar forcing data—also predicts the transition scale which is the lifetime of planetary-scale structures ($\tau_w \approx 8$ days); for the ocean, drifter data predict $\tau_{ow} \approx 1$ year, which is also close to observations.

To support the model further, we must examine extraterrestrial systems, here Mars. We extended the theory and predicted a transition at $\tau_w \approx 1.8$ sols. Comparison of terrestrial and Martian wind and temperature

spectra from both landers and reanalyses shows that the theory is remarkably successful in explaining the Martian statistics. In addition to our atmosphere and ocean, Mars thus provides a third example of a weather/macroweather transition. Since macroweather has fluctuations diminishing with increasing timescale (i.e., $H < 0$), then averages converge: on Mars too expect macroweather.

References

AchutaRao, K., and K. R. Sperber (2006), ENSO simulation in coupled ocean-atmosphere models: Are the current models better?, *Clim. Dyn.*, *27*, 1–15, doi:10.1007/s00382-006-0119-7.
Corrsin, S. (1951), On the spectrum of isotropic temperature fluctuations in an isotropic turbulence, *J. Appl. Phys.*, *22*, 469–473.
Diamond, H. J., et al. (2013), U.S. Climate Reference Network after one decade of operations: Status and assessment, *Bull. Am. Meteorol. Soc.*, *94*, 485–498.
Hasselmann, K. (1976), Stochastic climate models. Part I: Theory, *Tellus*, *28*, 473–485.
Hess, S. L., R. M. Henry, C. B. Leovy, J. A. Ryan, and J. E. Tillman (1977), Meteorological results from the surface of Mars: Viking 1 and 2, *J. Geophys. Res.*, *82*, 4559–4574, doi:10.1029/JS082i028p04559.
Hollingsworth, J. L., and J. R. Barnes (1996), Forced stationary planetary waves in Mars' winter atmosphere, *J. Atmos. Sci.*, *53*, 428–448.
Izakov, M. N. (2001), Turbulence and anomalous heat fluxes in the atmospheres of Mars and Venus, *Planet. Space Sci.*, *49*, 47–58, doi:10.1016/S0032-0633(00)00072-6.
Kolesnikov, V. N., and A. S. Monin (1965), Spectra of meteorological field fluctuations, *Izv. Atmos. Oceanic Phys.*, *1*, 653–669.
Leovy, C. (2001), Weather and climate on Mars, *Nature*, *412*, 245–249.
Lovejoy, S. (2013), What is climate?, *EOS*, *94*(1), 1–2.
Lovejoy, S. (2014), A voyage through scales, a missing quadrillion and why the climate is not what you expect, *Clim. Dyn.*, doi:10.1007/s00382-014-2324-0.
Lovejoy, S., and D. Schertzer (1986), Scale invariance in climatological temperatures and the local spectral plateau, *Ann. Geophys.*, *4B*, 401–410.
Lovejoy, S., and D. Schertzer (2010), Towards a new synthesis for atmospheric dynamics: Space-time cascades, *Atmos. Res.*, *96*, 1–52, doi:10.1016/j.atmosres.2010.01.004.
Lovejoy, S., and D. Schertzer (2011), Space-time cascades and the scaling of ECMWF reanalyses: Fluxes and fields, *J. Geophys. Res.*, *116*, doi:10.1029/2011JD015654.
Lovejoy, S., and D. Schertzer (2012), Low frequency weather and the emergence of the climate, in *Extreme Events and Natural Hazards: The Complexity Perspective*, Geophys. Monogr. Ser., vol. 196, edited by A. S. Sharma et al., pp. 231–254, AGU, Washington, D. C.
Lovejoy, S., and D. Schertzer (2013), *The Weather and Climate: Emergent Laws and Multifractal Cascades*, 496 pp., Cambridge Univ. Press, Cambridge, U. K.
Martinez, G. M., F. Valero, and L. Vazquez (2009), Characterization of the Martian convective boundary layer, *J. Atmos. Sci.*, *66*, 2044–2058, doi:10.1175/2009JAS3007.1.
Mitchell, J. M. (1976), An overview of climatic variability and its causal mechanisms, *Quat. Res.*, *6*, 481–493.
Monin, A. S. (1972), *Weather Forecasting as a Problem in Physics*, MIT Press, Boston, Mass.
Montabone, L., S. R. Lewis, and P. L. Read (2011), Mars Analysis Correction Data Assimilation (MACDA): MGS/TES v1.0, [Internet]. NCAS British Atmospheric Data Centre, 29 November., edited.
Newman, M. P., P. D. Sardeshmukh, and J. S. Whitaker (2003), A study of subseasonal predictability, *Mon. Weather Rev.*, *131*, 1715–1732.
Obukhov, A. (1949), Structure of the temperature field in a turbulent flow, *Izv. Akad. Nauk. SSSR. Ser. Geogr. I Geofiz*, *13*, 55–69.
Panofsky, H. A. (1969), The spectrum of temperature, *J. Radio Sci.*, *4*, 1143–1146.
Panofsky, H. A., and I. Van der Hoven (1955), Spectra and cross-spectra of velocity components in the meteorological range, *Q. J. R. Meteorol. Soc.*, *81*, 603–606.
Penland, C. (1996), A stochastic model of IndoPacific sea surface temperature anomalies, *Physica D*, *98*, 534–558.
Pinel, J., and S. Lovejoy (2014), Atmospheric waves as scaling, turbulent phenomena, *Atmos. Chem. Phys.*, *14*, 3195–3210, doi:10.5194/acp-14-3195-2014.
Pinel, J., S. Lovejoy, and D. Schertzer (2014a), The horizontal space-time scaling and cascade structure of the atmosphere inferred from satellite radiances, *Atmos. Res.*, *140–141*, 95–114, doi:10.1016/j.atmosres.2013.11.022.
Pinel, J., S. Lovejoy, and D. Schertzer (2014b), The horizontal space-time scaling and cascade structure of the atmosphere and satellite radiances, *Atmos. Res.*, *140–141*, 95–114, doi:10.1016/j.atmosres.2013.11.022.
Read, P. L., and S. R. Lewis (2004), *The Martian Climate Revisited: Atmosphere and Environment of a Desert Planet*, Springer, Chichester, U. K.
Sardeshmukh, P. D., and P. Sura (2009), Reconciling non-Gaussian climate statistics with linear dynamics, *J. Clim.*, *22*, 1193–1207.
Schertzer, D., and S. Lovejoy (1985), The dimension and intermittency of atmospheric dynamics, in *Turbulent Shear Flow*, edited by L. J. S. Bradbury et al., pp. 7–33, Springer, Berlin.
Tillman, J. E., L. Landberg, and S. E. Larsen (1994), The boundary layer of Mars: Fluxes, stability, turbulent spectra and growth of the mixed layer, *J. Atmos. Sci.*, *51*, 1709–1727.
Vallis, G. (2010), Mechanisms of climate variaiblity from years to decades, in *Stochastic Physics and Climate Modelling*, edited by P. W. T. Palmer, pp. 1–34, Cambridge Univ. Press, Cambridge, U. K.
Van der Hoven, I. (1957), Power spectrum of horizontal wind speed in the frequency range from 0.0007 to 900 cycles per hour, *J. Meteorol.*, *14*, 160–164.